JOURNAL OF MATERIALS SCIENCE 23 (1988) 3314–3320

Calorimetric measurements of transformation thermodynamics and thermal efficiencies of NiTi helices

A. P. JARDINE*
H. H. Wills Physics Laboratory, University of Bristol, Tyndall Avenue, Bristol, BS8 1TL, UK

The latent heats and thermal efficiency of a NiTi helix as the driving element of a Shape Memory Effect (SME) heat engine was measured by an adiabatic calorimeter capable of simulating a heat engine cycle. The latent heat measurements were found to be highly variable. Thermal efficiencies between 2.6 and 4.5% were measured in the limit of low external stresses needed for reproducible cycling behaviour.

1. Introduction

The thermal efficiencies of Shape Memory Effect (SME) heat engines have been a topic of some interest since the energy crisis in the early 1970s. Ironically, there have been no direct measurement of the thermal efficiencies. This is in part due to the difficulties in simulating a SME heat engine cycle in the calorimeter. Instead, estimates of the thermal efficiency based on an idealized heat engine cycle have been reported as the estimate can be calculated in terms of readily measured material parameters.

The thermodynamics of the SME are complex due to the stress dependence of the equilibrium transformation temperature T_0. The creation and growth of martensitic plates and their accompanying volume expansion creates variable internal stresses in a confined crystal such as a grain in a polycrystalline material, thus continually shifting the transformation temperature T_0. Salzbrenner [1] has demonstrated that T_0 is fundamentally indeterminant. Instead, four easily observable transformation temperatures are measured: M_s and M_f, the martensitic start and finish temperatures and A_s and A_f, the start and finish temperatures for austenite. These four temperatures are also stress dependent [2, 3]. The hysteresis present is a result of the elastic effects and can be measured as $A_f - M_f$; the transformation temperature region (TTR).

The ideal SME heat engine cycle can be described as follows (see Fig. 1). At M_f a single crystal rod is in a fully martensitic state, (assumed to be smaller in length than its high temperature phase), is loaded with load L. It is then heated to $A_f(\sigma)$ which drives the transformation back to its high symmetry austenitic state, causing the length to increase while doing work in raising the load. In this state the load L is removed. It is then cooled down to its fully martensitic state. The heat input into the rod is then

$$Q_{in} = \Delta H^{M\to A} + MC_p(A_f(\sigma) - M_f) \quad (1)$$

(i.e. the heat required to raise the mass from temperature M_f to $A_f(\sigma)$ plus the latent heat of transformation) and the work done is $\Delta l\, L$. The heat output on cooling is given by

$$Q_{out} = \Delta H^{A\to M} + MC_p(A_f - M_f) \quad (2)$$

The work done can be expressed as $W = Q_{in} - Q_{out}$ hence the thermal efficiency is

$$\eta_{th} = 1 - Q_{out}/Q_{in} \quad (3)$$

This result is completely general for any equilibrium phase transformation producing work, and does not depend on estimating T_0. Assuming that T_0 can be measured, it has been generally agreed [4–6] that the thermal efficiency for this cycle can be given as

$$\eta_{th} = \frac{\Delta H \Delta T_0}{T_0(C_p \Delta T_0 + \Delta H)} \quad (4)$$

where C_p is the specific heat of the material and $\Delta T_0 = T_0(\sigma) - T_0$. ΔH in the denominator may be a function of stress [6]. Equation 4 assumes 100% conversion of austenite into martensite, however this condition is never seen in NiTi and is likely never realized in any practical SME alloy. Hence, Equation 4 represents the maximum thermal efficiency that could be expected.

The microstructure observed on cooling through the transformation is a fraction of the material in the form of thin ellipsoidal plates of transformed martensite, surrounded by inert, untransformed austenite. In order to retransform to a fully austenitic structure, the martensitic transformation must work against internal friction and may also move surrounding inert material, as witnessed by macroscopic shape changes. Hence, even in the case of zero external load, work has been done and a thermal efficiency can be measured, designated as the "self-work" thermal efficiency.

Estimates in the literature for the thermal efficiencies for *fully loaded* (i.e. loaded to just before plastic deformation) SME heat engines based on Equation (4) vary from 4.5% to 21%, and vary widely even for the same material. Ahlers [4] considered single crystals of

* *Present address*: Department of Material Science and Engineering, Cornell University, Ithaca, NY 14853, USA.

0022–2461/88 $03.00 + .12

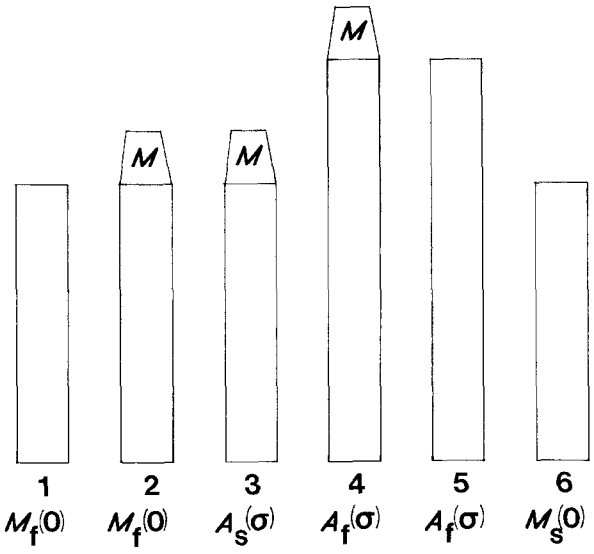

Figure 1 Thermodynamic cycle for an SME motor. An initially unstressed martensitic single crystal at temperature $M_f(0)$ (1) is stressed with negligible temperature and entropy changes (2). It is heated to $A_s(\sigma)$ (3) and then through the transformation to temperature $A_f(\sigma)$ doing work to lift the mass M. It is unloaded in (5) and allowed to cool to $M_s(0)$ (6). Further cooling allows a martensitic transformation to occur, arriving back at state (1), completing the cycle.

β-brass and arrived at a thermal efficiency of 4.9%. However, Tong and Wayman [5] arrived a thermal efficiency of 21% for Cu–36.0% Zn–1.75% Al alloy. Wollants *et al.* [6] found that in CuZnAl single crystals, thermal efficiencies of 10% may result if M_s is approximately 100 K. When the TTR occurs at room temperature, their estimates fall to 3% to 4%. Tong and Wayman [7] calculated a value of 4.5% for the thermal efficiency of a CuAlNi alloy.

Cunningham and Ashbee [8] calculated Carnot efficiencies of $\sim 20\%$ for NiTi and β-brass. They suggest 10% as a likely thermal efficiency on the grounds that heat engines, in general, are capable of realizing about one half of their Carnot efficiencies. For NiTi, Golestaneh [9] originally estimated a thermal efficiency of 15%, then in a subsequent paper, produced 4% [10]. Equation 4 was not used to produce this estimate and the validity of his initial calculations has been questioned [11].

The wide range of estimates demonstrates a need for a direct measurement of the thermal efficiency by observing the specific heat variation with temperature ($C_p(T)$), from which the thermal efficiency can be derived from Equations 1, 2 and 3. An unambiguous estimate for the thermal efficiencies of SME alloys can be obtained as T_0 is not estimated.

The thermal efficiency of stoichiometric NiTi was investigated, due to its high (room temperature) transformation, relative ease of setting a preferred shape when the material is above the transformation temperature; these material characteristics are complemented by general scientific and industrial interest in the material.

The transformation from the high symmetry, high temperature (B2) phase normally goes to the martensitic low symmetry B19 phase, however the occurrence of a competing transformation at the same temperature to an intermediate rhombohedral (R) phase in NiTi complicates the overall transformation thermodynamics. Additional transformation paths are B2 → R and R → B19 or both. This transformation is not a precursor to the martensitic transformation but is an independent transformation [12] complete with its own memory effect [13, 14]. The R phase is generally not observed in stoichiometric NiTi, however constrained ageing [14], annealing after cold working [15] and ageing at intermediate temperatures [16] have been demonstrated to enhance this transformation.

Using a specially designed adiabatic calorimetry, the engine cycle described above was directly measured for NiTi. The specific heat anomalies through the transformation were measured by Berman *et al.* [17] for the martensite to austenite transformation in polycrystalline NiTi and observed a non-repeatable, broad specific heat peak; the broadness is due to the continuously changing elastic energy. Variations in peak broadness were attributed partly to continually changing elastic energy and partly to variable internal stress.

It is observed that stressing the material to just before plastic deformation would result in degradable cycling, due to additional dislocation generation [18] creating work-hardening. Indeed there seems to be a correlation between loading stress and cycle lifetime of the material. For reproducible results over a large number of cycles, the stresses to be applied have to be small, though this lowers the efficiencies and hence the power-weight ratios of the engines.

Repeatable efficiencies can then be considered to be the efficiency as the external stress vanishes, i.e. the "self work" thermal efficiency. Even this may be dubious if the coherence between the parent and martensite is poor, as thermal cycling may then produce misfit dislocations.

2. Calorimeter description

The relevant aspects of the calorimeter are reviewed here however a complete description has been given elsewhere [19]. The adiabatic calorimeter consisted of two coaxial copper cylinders wound with copper heater wire, to produce a well defined thermal environment for the sample (Fig. 2). These cylinders were in a stainless steel vacuum chamber at a pressure of 10^{-6} torr, and were supported from below by Bakelite rods mounted on a Bakelite platform. The unique feature of this calorimeter was that the sample (a NiTi helix) was suspended by thin stainless wires from a moveable hook and could be loaded by suspending a weight from similar wires wrapped around the bottom. These wires were run out of the calorimeter cavity through holes in the can, to either the top suspension hook or to the bottom weight system.

Heater wires were run around the wire so that they did not restrain expansion of the helix. Chromel–alumel thermocouples were attached to the sample and this assembly was then wrapped in aluminium foil to provide an adiabatic environment. The inner can temperature was measured by a four-terminal platinum wire thermometer. A Tecmar A/D D/A board on a Z80 microcomputer was used to provide temperature measurement and control.

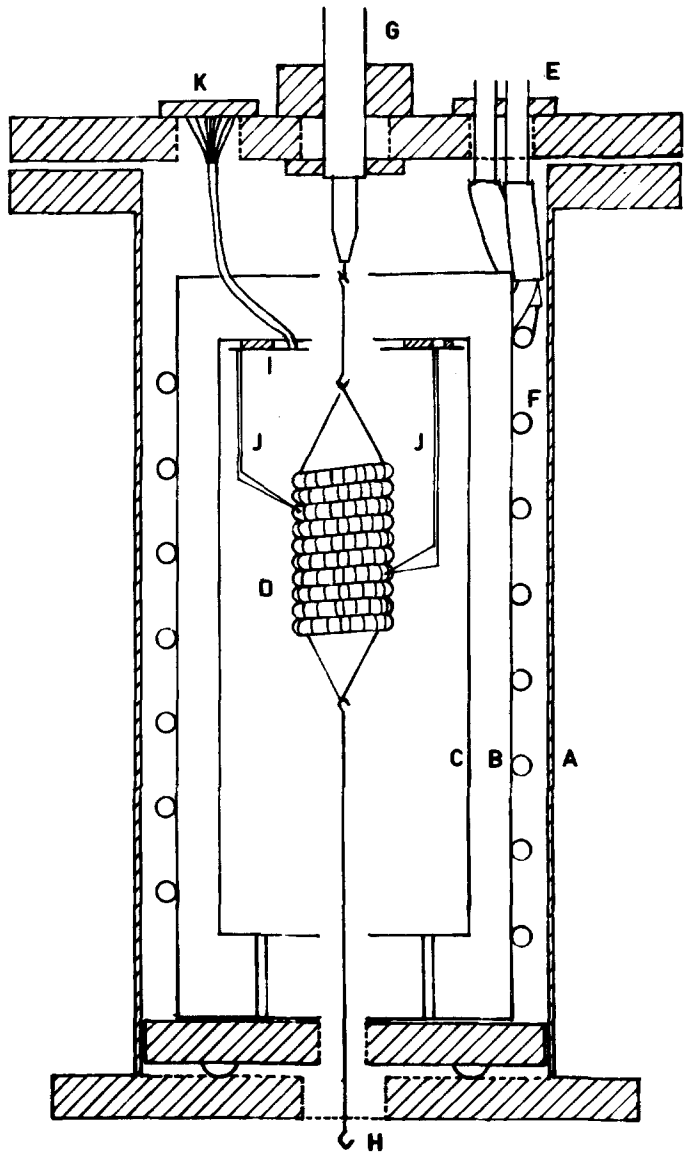

Figure 2 The calorimeter is composed of a vacuum-tight can (A), containing an adiabatic shield (B) and reference shield (C) which encloses the sample (D). The adiabatic shield is cooled by running liquid nitrogen or cold water from (E) to the cooling coil (F). The sample is suspended by thin wire from the adjustable rod assembly (G) and can be stressed by adding weights at (H). The electronic transducers are attached thermally to the reference shield at (I), with thermocouples (J) running to the sample. Power and signal lines are connected to external apparatus by two ports, one of which is shown (K).

For heating, the mode of operation that was most successful was to run a fixed current through the sample while keeping the inner sample temperature constant. For cooling, the inner cylinder was cooled to liquid nitrogen temperatures and the sample was allowed to cool from its fully austenitic state while its temperature was monitored. From the measurements of the sample temperature with time, mass, and input power, $C_p(T)$ could be calculated (and so the sample entropy $S(T)$). The power output on cooling was estimated from the radiation power losses given by Boltzmanns' law, but a more refined estimate can be made by matching C_p data for cooling to heating data.

As-received, 3 mm diameter 50.0 at% Ni–Ti wire samples supplied by Raychem Corp. were prepared by initially annealing at 500° C to soften the wires so that they could be wound around a $\frac{3}{4}''$ ($1'' = 2.54$ cm) mandril at a pitch of 3 turns per inch. Samples are then clamped into position by grub screws and reannealed at 500° C for one hour followed by furnace cooling. Thermocouples were then attached to the sample and wound parallel to, but not touching, the bifilarily wound heating wire to ensure good thermal contact of the thermocouple with the sample. Thermocouples were prepared by first putting a thin amount of varnish onto the junctions to ensure that there was no electrical contact to the sample. (During the transformation, Wang and Beuhler [20] observed that a variable e.m.f. occurs through the TTR.) Good thermal contact was ensured by clamping the thermocouple to the surface using thin nickel wire and then applying a thin layer of heat sink compound on the junction. The assembly was held in place with a small amount of epoxy. Finally, a small piece of aluminium foil was put on the thermocouple to minimize radiation losses to the reference shield. An example of such a prepared sample is shown in Fig. 3.

The thermal time constant for the non-transforming NiTi spring system was estimated as follows. The specific heat for non-transforming NiTi at 300 K is approximately $0.50\,J\,g^{-1}\,K^{-1}$. The spring mass was typically 30 g, so the thermal capacitance of the sample is then $15\,J\,K^{-1}$. The length of the bifilarily wound heating wire was 126 cm and had a diameter of approximately 0.13 cm, so the total area of contact (A) is then $16.4\,cm^2$. The heating wire was wrapped in cotton of approximate thickness (l) of 0.01 cm and has a thermal conductivity (κ) of $0.03\,W\,m^{-1}\,K^{-1}$. For a 1° C temperature difference then the heat transferred is given by

$$Q = \kappa A \Delta T / l \qquad (5)$$

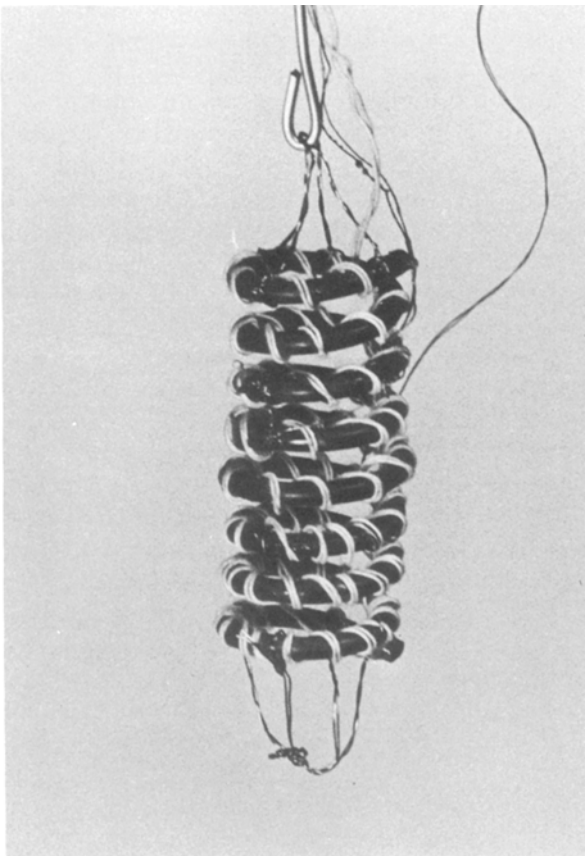

Figure 3 Typical heating configuration for the sample. The helix is suspended from a 0.16 cm diameter stainless steel rod by thin insulated nickel wire. The cotton-covered bifilarily wound heater wire is wrapped around the helix such that the SME helix can expand without being constrained by the heater. Also seen to the right of the picture are two lagged thermocouples. The insulated copper wire at the bottom of the helix can be attached to a second stainless steel hook, from which weights can be suspended. The helix has an axial length of 6.2 cm.

substituting in the values gives $Q = 0.492\,\mathrm{W\,K^{-1}}$. Therefore $R_{th} = 2.033\,\mathrm{K\,W^{-1}}$ and so the thermal time constant is $R_{th}C_{th} = 30\,\mathrm{sec}$.

Typical heating rates were 1.2 to 2.8 K $\mathrm{min^{-1}}$ which indicates that the samples were thermally equilibrated with the input power used. Lower heating rates were attempted but it was found that the power losses to the walls of the calorimeter were large enough to prevent heating. The heating rates used were the lowest possible with this calorimeter.

4. Latent heat measurements

Table I shows the results of the entropy and enthalpy changes calculated from heating one air cooled NiTi helix. The latent heats are surprisingly large as these values are comparable and in some cases larger than latent heats observed in steels. Rapid pulse calorimetry performed by Mercier and Melton [21] gave $\Delta S^{M\to A}$ as $0.071\,\mathrm{J\,g^{-1}\,K^{-1}}$ for stoichiometric polycrystalline NiTi wire which is consistent with the values obtained. It is evident that there are large variations in the results for one sample. The errors for the specific heats and entropy values are small compared to these variations. The magnitude of these variations are similar to those reported by Berman *et al.* [17].

TABLE I Enthalpy and entropy data for one NiTi Helix. The value of T_0 is calculated from $\Delta H = T_0 \Delta S$.

$\Delta H^{M\to A}$ ($\mathrm{J\,g^{-1}}$)	$\delta(\Delta H^{M\to A})$ ($\mathrm{J\,g^{-1}}$)	ΔS ($\mathrm{J\,g^{-1}\,K^{-1}}$)	$\delta(\Delta S^{M\to A})$ ($\mathrm{J\,g^{-1}\,K^{-1}}$)	T_0 (K)
22.5	4.9	0.069	0.015	326.3
36.5	5.6	0.111	0.017	331.2
30.7	6.1	0.091	0.018	337.1
29.3	4.9	0.089	0.015	329.6
46.7	6.7	0.139	0.020	336.3
14.2	3.6	0.044	0.011	331.5
19.6	1.3	0.060	0.004	319.5
12.8	3.2	0.040	0.010	319.5
19.0	4.9	0.058	0.015	327.7
26.6	3.7	0.081	0.016	328.6
28.1	3.7	0.084	0.011	334.2
26.9	4.0	0.081	0.012	332.3
24.5	4.0	0.074	0.012	330.5

5. Possible causes for observed variations

The high temperature state of all the runs are the same as they are entirely β phase. Suppose the low temperature state of the sample may not be consistent for all runs despite being cooled slowly in the calorimeter. With a variable fraction to martensite to retransform, the latent heats must be smaller. There would then be a correlation between the starting temperature and the measured latent heat of transformation, however no discernable correlation was observed. This hypothesis is also unlikely as the martensite does transform isothermally below M_s so that the time between runs should allow complete transformation.

There were also no correlations between heating rate and $\Delta S^{M\to A}$, hence it would appear that these variations are real and not due to a systematic error.

Suppose variable amounts of differing types of martensite form on cooling from the high temperature β phase. In NiTi, Wasilewski [22] noticed that two types of martensitic microstructure are formed on heating from a partially cooled state; that formed by quench inducing (QIM, denoted as γ'), and that formed by stress inducing (SIM, denoted β'). Possible transformation routes between low and high temperature states are then

$$\beta' \rightarrow \beta$$
$$\gamma' \rightarrow \beta' \rightarrow \beta$$
$$\gamma' \rightarrow \beta$$

Golstaneh [10] states that β' and γ microstructure would have latent heats of transformation which would differ by the work required to create the β'. There is no external stress applied on cooling, the cooling process is similar in all cases, and the external loads applied on heating are $\sim 10\%$ of the load required for plastic deformation, hence the amount of stress-induced martensite would likely be small and would not furnish enough deviation in latent heat to account for the observed variations.

5.1. Influence of a secondary peak

The appearance of a small secondary peak at ~ 311 K observed in some experiments was investigated (Fig. 4). It was noticed that these peaks are of variable enthalpy. The small peaks, all of which started at 307 K and

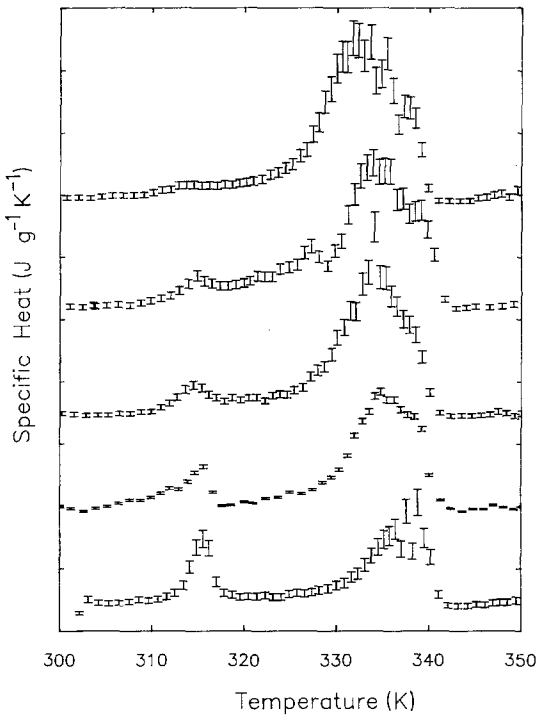

Figure 4 The influence of pre-austenitic peak at 313 K tends to decrease the magnitude of the austenitic latent heat.

finished at 315 K, were more consistent than the major specific heat anomalies. A linear regression analysis of the enthalpy change of this peak (ΔH^R) against the enthalpy change of the large austenitic peak ($\Delta H^{M\to A}$) in Fig. 5 gave

$$\Delta H^{M\to A} = -4.56\,\Delta H^R + 20.78 \qquad (6)$$

with a root mean square deviation of 1.1 J g^{-1} in the slope. There were no evident correlations between the size of the secondary peak and any of the conditions of the experiment; for example, no correlations between ΔS_R and heating rate, initial temperatures, sample history, etc. These peaks were not observed in all experiments; it may be that the algorithm for computing the specific heat is insufficiently sensitive to resolve this contribution. From the error analysis, C_p is known to be ± 0.05 J g^{-1} K^{-1}. Taking a temperature transformation range of 8 K for B19 → R then the latent heat for an undetected pre-austenitic anomaly could be as large as 0.8 J g^{-1}, hence the maximum variation to $\Delta H^{M\to A}$ could only be 1.8 J g^{-1}; not enough to explain the magnitude of the variations.

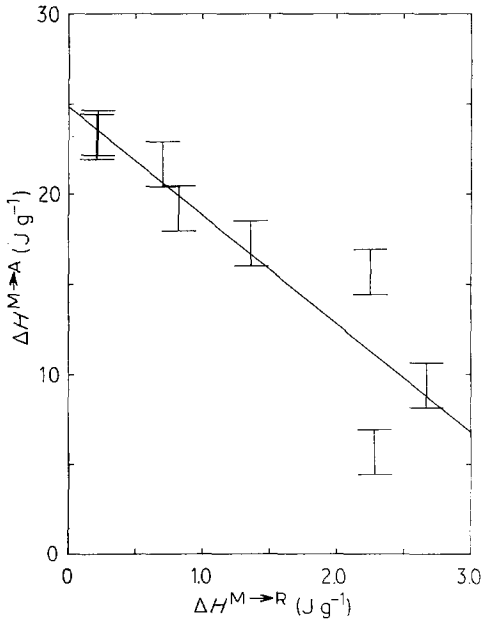

Figure 5 There is an evident correlation between the latent heats of the pre-austenitic peaks at 313 K and the large austenitic peak.

There is some corroborative evidence that the secondary peak is associated with the "R" phase. A premartensitic peak is frequently observed on cooling in DSC [12] and TEM [24] although a preaustenitic peak has never been observed in TEM. In a forthcoming paper, Jardine *et al.* [16] presented evidence from DSC of a preaustenitic anomaly in similarly prepared NiTi where the relative magnitudes of the two peaks on heating are consistent with those observed here. It seems likely that the secondary peak is due to the R phase.

The observed linear relationship between ΔH^R and $\Delta H^{M\to A}$ may be that by transforming via the R-phase from the martensite to austenite, there may be less energy required, analogous to a catalytic reaction. Linearity may be a consequence of differing amounts of martensite able to transform via the R-phase to austenite.

Why one sees the R-phase peak in some cases and why there are varying amounts of differing martensites may be due to differing, highly sensitive, irreproducible thermoelastic conditions created on cooling. As these alloys have a preferred hot shape but no preferred cold shape, it is likely that the initial plate would nucleate at a position dependent on the local thermal and elastic conditions which may differ from cycle to cycle. The positions of sequential nucleations will be dependent on the position of the first plate. Thus the martensitic plates would form in a random manner such that the distribution which would not likely be the same as previous distributions. This "chaotic" behaviour would probably be severely reduced in the presence of an external stress, which would dominate the local thermoelastic conditions. This situation occurs in stress-induced martensite, where values of ΔH deduced from a Clapeyron relationship are repeatable [25]. It would be interesting to repeat the experiments on SME alloys with two-way shape memory (i.e. preferred hot and cold shapes). In this case, plates would not form in a random fashion so that the latent heat measurements should not be as variable.

6. Thermal efficiency determination

Simulation of the engine cycle described in the introduction is performed. In the martensitic state, a load is applied to the sample. As the elements are helical, this result in a distribution of stress across a section of the helix. The helix is then heated to a fully austenitic state and subsequently unloaded. The helix is then allowed to cool to its martensitic state.

To measure the thermal efficiency of this cycle, C_p data for both heating and cooling is required. Cooling was accomplished primarily through radiative transfer from the sample to the shield. By cooling the adiabatic shield down to liquid nitrogen temperatures, the reference shield temperatures could be brought

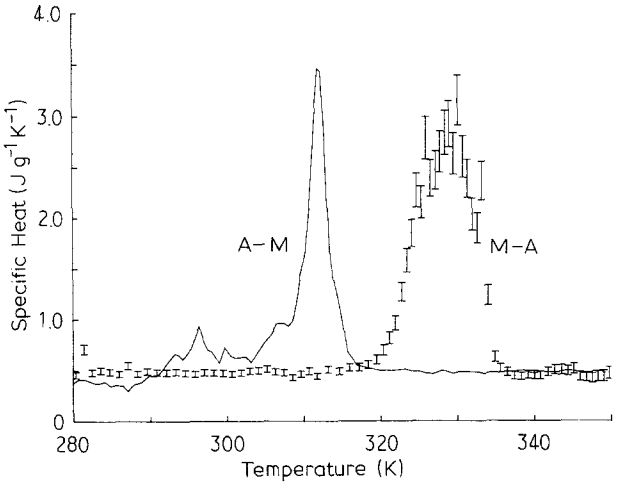

Figure 6 The heating and cooling curves for an air-cooled NiTi helix. During heating, the sample was loaded with a 400 g load, which was removed before heating. The cooling curve shows a sharper C_p peak than in the heating case.

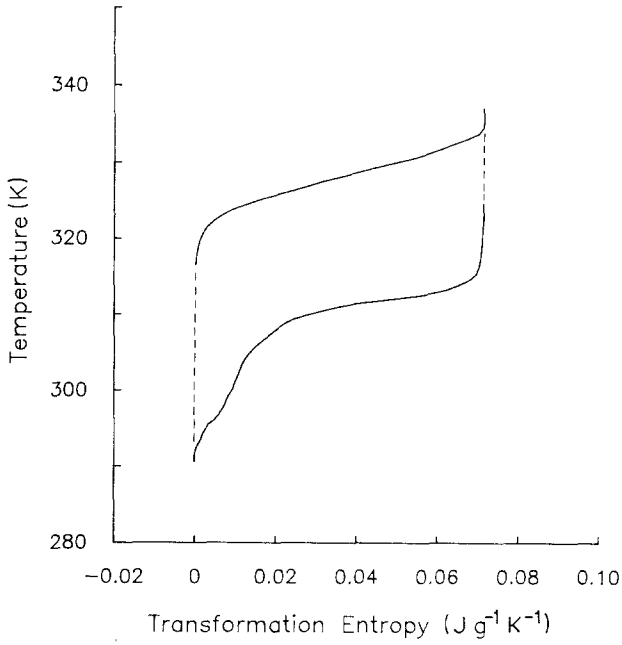

Figure 7 The *TS* plot generated from the C_p data. The cooling data was scaled so that the net entropy over the cycle was zero.

down to $-10°$ C. Cooling curves obtained showed a sharp well defined martensitic peak (Fig. 3). It is observed that the A_s temperature is below M_s, consistent with thermoelastic transformations.

The measurement of C_p on cooling is more difficult due to (a) our apparatus was found to be difficult to provide adequate cooling rates to the sample and (b) the input power on cooling, the radiative power loss, is difficult to estimate from the sample temperature decay profile. Cooling curves were initially calculated by Stephan's law,

$$P = C(T_s^4 - T_{ref}^4), \quad (7)$$

after estimating the radiative power loss constant (C). The difficulty in measuring cooling input power can be overcome by noting that in a *TS* plot for an engine cycle, the change in entropy over one cycle must be approximately zero. Any non-equilibrium contributions to the cycle which would allow for deviation from this condition are assumed small.

The initial C_p cooling curve was fitted to the heating curve C_p so that the entropy values at the initial and final points of the cycle were zero. Any discrepancy between initial and final entropy states as calculated from

$$\Delta S = \int (C_p/T)\, dT \quad (8)$$

were ascribed to the selection of cooling input power constant. This constant was recalculated so that the net entropy per cycle was zero. This method could be checked by comparing the latent heat for the transformation as calculated from this method compared to values obtained elsewhere.

In Fig. 6 are shown the heating (loaded) and cooling (unloaded) $C_p(T)$ curves of one air cooled sample. The entropy changes and temperature changes on loading and unloading could not be directly measured in our apparatus, however the temperature [8] and entropy [6] changes for adiabatic loading and unloading for small loads have been shown to be negligible. The resultant *TS* plot is shown in Fig. 7. The area contained by the closed curve then gives the work done. The area under the top curve in Fig. 7 gives Q_{in} and the area under the bottom curve gives Q_{out}. The values for Q_{in} and Q_{out} were calculated directly from the specific heat using Equations 1 and 2. The efficiencies are easily calculated from Equation 3.

Due to difficulties in getting adequate cooling rates, only a few complete engine cycles were obtained. The data taken was for one air cooled NiTi helix which gave efficiencies of 3.1% and 4.2% for a load of 400 g. In both cases the latent heat of transformation on cooling $\Delta H^{A\to M}$ produces values of 25 J g^{-1}, consistent with those measured from stress–strain data [25]. These values for η_{th} represent the minimal efficiencies and hence the most reproducible on the long term cycling.

As the values for latent heats calculated for the cooling data were reasonable, thermal efficiency calculations were performed for the other specific heat data obtained for heating. Data displaying the pre-austenitic anomaly were disqualified from the thermal efficiency calculations, due to possible unknown nature of their state prior to transformation. The single peak data used for the generation of results ensure that initial and final states are the same. The thermal efficiencies calculated for the single peak results are calculated and displayed in Table II.

Thermal efficiencies from 2.7% to 4.1% were calculated which represent at best about 8% of the Carnot efficiency (taking T_h as 444 K and T_c as 292 K). With

TABLE II The thermal efficiencies for "one peak" results on polycrystalline NiTi helices as calculated from the method discussed in Section 6. The values tend to be in the range of 3 to 4% representing the "self-work" thermal efficiency.

$\Delta H^{M\to A}$ (J g^{-1})	$\Delta H^{A\to M}$ (J g^{-1})	η_{th} (%)	$\Delta S^{M\to A}$ (J g^{-1} K^{-1})	Load (g)
22.6	21.4	2.7	0.069	0
36.5	34.2	3.8	0.111	0
30.7	28.4	4.1	0.092	400
29.3	27.6	3.1	0.089	400
26.6	25.0	3.2	0.081	800
28.1	26.0	3.8	0.084	800

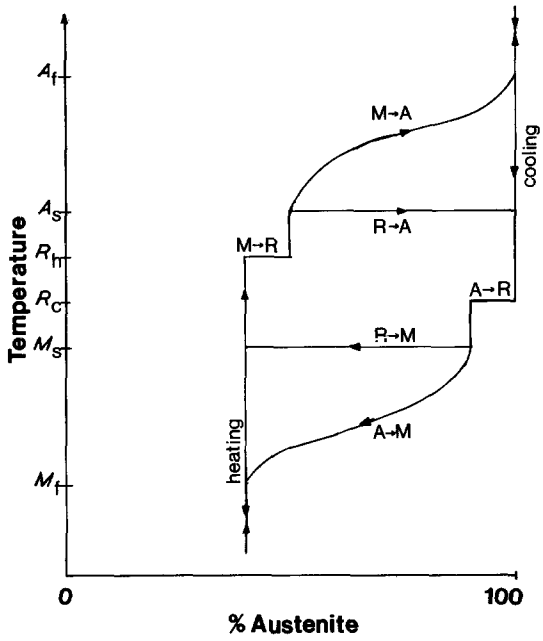

Figure 8 Proposed model of transformation routes available in NiTi. On cooling, a fraction of the B2 transforms to R at R_c and another fraction begins to transform to B19 at M_s, with the reaction complete at M_f. The R phase will also transform to B19 (shown here at M_s). Some fraction of the B2 will remain untransformed. A similar set of transformations occurs on heating.

larger loads the thermal efficiencies will become greater as more work is done. Masses of either 400 g or 800 g loaded the samples when heated, which does not introduce a significant amount of stress, but enough to demonstrate that work was being performed. A load of 800 g created a maximum stress of 16 MPa in the helix which is small compared to the maximum stress of 300 MPa [16] which can be applied before plastic deformation. No correlation was found between ΔH and applied load, possibly indicating that the internal work done by the sample in retransforming back to the austenite is much larger than the work done in raising the loads.

7. Discussion

The thermodynamics of the SME in NiTi are clearly complicated. There is a strong correlation between ΔH^R and $\Delta H^{M\rightarrow A}$ which is an interesting result and correlates to previous work of a possible R-phase anomaly observed as a pre-austenitic specific heat anomaly [16].

Thermal efficiencies of 3% to 4% were measured for the engine cycle and efficiencies of 2.5 to 4% were calculated for the other heating data by matching the cooling curves obtained with this data. These values agree; the variability in these values is due to the variations in $C_p(T)$ between cycles. These represent the minimal efficiencies to be expected. The variation in $C_p(T)$ in turn may be due to the variations in martensitic plate distribution from varying local thermoelastic conditions on cooling.

For long term cycling of the elements in an engine, the elements will necessarily need to be loaded to much less than their elastic limit to avoid the generation of dislocations which will impair and ultimately stop the device performance, hence these results are relevant to the technologist as well as to the physicist.

Transformation routes can be summarized in Fig. 8. Heating from $T < M_f$ the martensite can take two different routes to transform to austenite, one by going directly to austenite and the other via the R-phase transformation. It seems that the amount of material going by the latter path is dependent on highly sensitive thermoelastic conditions, based on the highly variable amounts of R-phase observed. On cooling, some fraction of the austenite transforms via the R-phase and another fraction of the remaining material transforms to martensite. Below M_f there will be some untransformed austenite.

Further calorimetric investigations supplemented by TEM microstructural investigations are needed to investigate the variability of the C_p data.

Acknowledgements

The author is grateful to the British Gas Corporation for a British Gas Scholarship and wishes to thank Mr H. N. Young for construction of the calorimeter. I am also grateful to Dr Jeff Sargent for helpful technical discussions and assistance. This work was carried out under the supervision of Professor K. H. G. Ashbee.

References

1. R. J. SALZBRENNER and M. COHEN, *Acta Metall.* **24** (1980) 739.
2. H. POPS and N. RIDLEY, *Met. Trans.* **1** (1970) 2653.
3. R. J. WASILEWSKI, *ibid.* **2** (1971) 2973.
4. M. AHLERS, *Scripta Metall.* **9** (1975) 7174.
5. H. C. TONG and C. M. WAYMAN, *Acta Metall.* **22** (1974) 987.
6. P. WOLLANTS, P. M. de BONTE and J. ROOS, *Z. Metallkde* **70** (1979) 113.
7. H. C. TONG and C. M. WAYMAN, *Scripta Metall.* **9** (1975a) 757.
8. B. CUNNINGHAM and K. H. G. ASHBEE, *Acta Metall.* **25** (1977) 1315.
9. A. A. GOLSTANEH, *J. Appl. Phys.* **49** (1978) 1241.
10. *Idem., Acta Metall.* **28** (1980) 1427.
11. H. MOHAMMED and R. BANKS, *J. Appl. Phys.* **50** (1978) 6029.
12. E. GOO and R. SINCLAIR, *Acta. Metall.* **33** (1985) 1717.
13. H. C. LING and R. KAPLOW, *Met. Trans* **11A** (1980) 77.
14. T. HONMA, M. NISHIDA and T. HOMNA, *J. de Phys.* **43** (1982) C4-225.
15. S. MIYAZAKI, Y. OHMI, K. OTSUKA and Y. SUZUKI, *J. Physique,* **43** (1982) C4–255.
16. A. P. JARDINE, K. H. G. ASHBEE and M. BASSETT, *J. Mater. Sci.* (1988) to be published.
17. H. A. BERMAN, E. D. WEST and A. G. ROZNER, *J. Appl. Phys.* **38** (1967) 4473.
18. R. KOPA, Proceedings NiTi Heat Engine Conference, Silver Spring, MA, NSWC MP 79-448, edited by D. M. Goldstein and L. J. McNamara, US Dept. of Navy (1979) 8-1.
19. A. P. JARDINE, *Rev. Sci. Instron.* **59** (1988) A. P. Jardine, PhD thesis, University of Bristol, Bristol (1986).
20. F. E. WANG and W. J. BUEHLER, *Appl. Phys. Lett.* **21** (1972) 105.
21. M. MELTON and O. MERCIER, *J. Appl. Phys.* **50** (1979) 5747.
22. R. J. WASILEWSKI, *Met. Trans.* **2** (1971) 2973.
23. R. J. WASILEWSKI, S. R. BUTLER, J. E. MANLON and D. WARDEN, *Met. Trans.* **2** (1971) 229.
24. C. M. HWANG, M. MEICHLE, M. B. SALOMAN and C. M. WAYMAN, *Phil. Mag.* **A47** (1983) 9, 31, 177.
25. A. P. JARDINE, *J. Mater. Sci.* **23** (1988) 3314.

Received 22 September 1987
and accepted 26 January 1988